Crystallographic and Biochemical Analysis of Cocaine-Degrading Antibody 15A10[†,‡]

N. A. Larsen,[⊥] P. de Prada,[§] S.-X. Deng,[§] A. Mittal,[§] M. Braskett,[§] X. Zhu,[⊥] I. A. Wilson,*[,⊥,∥] and D. W. Landry*[,§,▽]

The Department of Molecular Biology and Skaggs Institute for Chemical Biology, The Scripps Research Institute, La Jolla, California, and The Department of Medicine, Columbia University, College of Physicians and Surgeons, New York City, New York

Received March 14, 2004; Revised Manuscript Received April 26, 2004

ABSTRACT: Catalytic antibody 15A10 hydrolyzes the benzoyl ester of cocaine to form the nonpsychoactive metabolites benzoic acid and ecgonine methylester. Here, we report biochemical and structural studies that characterize the catalytic mechanism. The crystal structure of the cocaine-hydrolyzing monoclonal antibody (mAb) 15A10 has been determined at 2.35 Å resolution. The binding pocket is fairly shallow and mainly hydrophobic but with a cluster of three hydrogen-bond donating residues (TrpL96, AsnH33, and TyrH35). Computational docking of the transition state analogue (TSA) indicates that these residues are appropriately positioned to coordinate the phosphonate moiety of the TSA and, hence, form an oxyanion hole. Tyrosine modification of the antibody with tetranitromethane reduced hydrolytic activity to background level. The contribution from these and other residues to catalysis and TSA binding was explored by site-directed mutagenesis of 15A10 expressed in a single chain fragment variable (scFv) format. The TyrH35Phe mutant had 4-fold reduced activity, and TrpL96Ala, TrpL96His, and AsnH33Ala mutants were all inactive. Comparison with an esterolytic antibody D2.3 revealed a similar arrangement of tryptophan, asparagine, and tyrosine residues in the oxyanion hole that stabilizes the transition state for ester hydrolysis. Furthermore, the crystal structure of the bacterial cocaine esterase (cocE) also showed that the cocE employs a tyrosine hydroxyl in the oxyanion hole. Thus, the biochemical and structural data are consistent with the catalytic antibody providing oxyanion stabilization as its major contribution to catalysis.

The powerful reinforcing effects of cocaine have been linked to its action in the mesolimbocortical reward pathway, where cocaine inhibits nerve terminal reuptake of the neurotransmitter dopamine (*1*). Development of suitable cocaine antagonists as therapeutics for cocaine abuse and addiction have foundered on the difficulties inherent in inhibiting an inhibitor (*2*). As an alternative to small molecule blockade in the central nervous system (CNS), we considered the possibility of peripheral blockade, that is, enhanced degradation of cocaine in the peripheral circulation preventing cocaine from reaching its receptors in the CNS (*3*−*5*). Hydrolysis of the benzoyl ester of cocaine (Figure 1) is an ideal degradation path because the resulting products are nonreinforcing and nontoxic.

Catalytic antibodies are a class of artificial enzymes with unique potential as therapeutic agents for cocaine addiction (*3*). Moreover, ester hydrolysis is the most studied of the antibody-catalyzed reactions (*6*, *7*). The most common mechanism for antibody-catalyzed ester hydrolysis relies on the stabilization of the tetrahedral oxyanionic transition state, although additional contributions to catalysis have been reported (*8*−*10*). Murine catalytic antibody 15A10 was elicited from a phosphonate monoester transition state analogue of cocaine coupled to bovine serum albumin (BSA)[1] (Figure 1). 15A10 hydrolyzes the benzoyl ester of cocaine to yield the nonpsychoactive metabolite ecgonine methylester (Figure 1) with a k_{cat} of 2.3 min^{-1}, K_M of 220 μM, and $k_{cat}k_{uncat}^{-1} = 2.3 \times 10^4$ (Table 1). The K_i for the transition state analogue is ∼10 nM implying binding energy has been converted to catalysis ($K_M K_{DTSA}^{-1} \approx k_{cat}k_{uncat}^{-1}$), as has been inferred for a number of other hydrolytic antibodies (Table 1) (*11*).

Characterization of 15A10 shows little product inhibition by structurally related, but pharmacologically inactive,

[†] Support was provided by the Office of National Drug Control Policy/Counter Drug Assessment Center (DWL), the National Institutes of Health (to I.A.W., Grant GM38273) and the Skaggs Institute (to N.A.L.).

[‡] The atomic coordinates and structure factors for the 15A10 Fab have been deposited in the RCSB Protein Data Bank with accession code 1NJ9.

* To whom correspondence should be addressed.

[⊥] The Scripps Research Institute.

[§] Columbia University.

[∥] Phone: (858)-784-9706. Fax: (858)-784-2980. E-mail: wilson@scripps.edu.

[▽] Phone: (212)-305-2131. Fax: (212)-305-1152. E-mail: dwl1@columbia.edu.

[1] Abbreviations: mAb, monoclonal antibody; TSA, transition state analogue; scFv, single-chain fragment variable; cocE, cocaine esterase; BSA, bovine serum albumin; LD, lethal dosage; Fab, fragment antigen binding; IgG, immunoglobulin G; Fc, fragment crystallizable; RMS, root-mean-square; PBS, phosphate-buffered saline; V_H, variable heavy; V_L, variable light; PCR, polymerase chain reaction; NCS, noncrystallographic symmetry; CDR, complementarity-determining region.

10.1021/bi049495l CCC: $27.50
Published on Web 06/03/2004

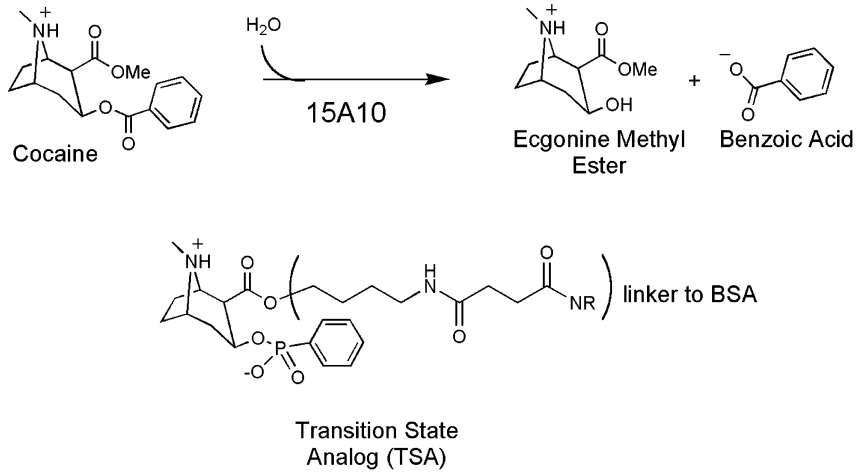

FIGURE 1: 15A10 Transition state analogue. 15A10 hydrolyzes cocaine to ecgonine methylester and benzoic acid and was originally elicited from the transition state analogue coupled to BSA. TSA-1 corresponds to TSA with the linker replaced with a single methyl group.

Table 1: Kinetic Parameters for Esterolytic Antibodies with Known Crystal Structures

antibody	pH[a]	$k_{cat}K_M^{-1}$ [b] (min^{-1} M^{-1})	k_{cat} [b] (min^{-1})	K_M [b] (μM)	$K_MK_{DTSA}^{-1}$ [b]	$k_{cat}k_{uncat}^{-1}$ [b]	ref
15A10	8.4	1.0×10^4	2.2	220	2.2×10^4	2.3×10^4	*4*
D2.3	8.3	1.3×10^4	3.6	280	1.1×10^5	1.3×10^5	*51*
43C9	9.3	2.8×10^7	1500	54	6.8×10^4	2.7×10^4	*56*
48G7	8.2	1.4×10^4	5.5	390	8.7×10^4	1.6×10^4	*57*
17E8	8.7	4.8×10^5	220	460	0.9×10^3	8.3×10^3	*49*
CNJ206	8.0	3.5×10^3	0.4	80	0.7×10^2	1.6×10^3	*50*
6D9	8.0	2.9×10^3	0.1	50	0.9×10^3	0.9×10^3	*52*

[a] Experimental pH at which kinetic parameters are tabulated. [b] k_{cat} and K_M are the Michaelis−Menten parameters, k_{uncat} is the first-order rate constant for background hydrolysis, and K_{DTSA} is the dissociation constant for the transition state analogue.

cocaine metabolites benzoylecgonine, ecgonine methylester, and ecgonine but was inhibited by benzoic acid with K_i = 250 μM (Figure 1) (*4*). These metabolites are derived from enzyme-mediated hydrolysis in the bloodstream and liver, which together account for the ~30 min in vivo half-life of cocaine. Passive administration of 15A10 attenuated the reinforcing effects of cocaine in a rat model for cocaine abuse (*5*, *12*), and pretreatment with 15A10 served as an antidote for seizures and lethality in a dose-dependent fashion after a LD_{90} infusion of cocaine (*5*). The potential for this therapeutic would be enhanced by improved kinetic parameters, manifested as either a lower K_M or a higher k_{cat}. A lower K_M would be especially desirable, since the antibody would be operating under subsaturating conditions at cocaine concentrations typically found in a user (~1 μM in the peripheral circulation (*13*) and ~30 μM in the pulmonary circulation for smoked crack-cocaine (*4*)).

Improvement of catalytic proficiency would be advantageous in a clinical setting for treatment of cocaine addiction and for emergency detoxification. Toward this end, the crystal structure of the unliganded Fab 15A10 was determined at 2.35 Å resolution (*14*). The binding pocket of 15A10 differs significantly from cocaine-binding antibody GNC92H2 (*15*). Structural analysis and docking of the transition state analogue in the binding pocket of 15A10 reveal a putative oxyanion hole composed of TrpL96, AsnH33, and TyrH35. Mutation of these residues results in partial or complete loss of catalytic activity. Interestingly, the configuration of the oxyanion hole is similar to that seen in the bacterial cocaine-hydrolyzing enzyme, cocE (*16*). The crystal structure provides a foundation for mutagenesis to enhance catalytic proficiency and for additional antibody humanization (*17*).

MATERIALS AND METHODS

Crystallization, Structure Determination, and Refinement. Details of protein preparation, structure determination, and refinement are published elsewhere (*14*). In brief, IgG was obtained from cultured hybridoma cells and digested with papain to Fab and Fc fragments. The Fab was purified by protein A and protein G affinity chromatography, concentrated to 20 mg ml^{-1} in 0.2 M sodium acetate buffer, pH 5.5, and crystallized (*14*). Crystals diffracted to 2.35 Å resolution, and the structure was determined by molecular replacement using EPMR (*18*). Although the data were twinned, the structure was successfully refined using SHELXL (*19*) and CNS (*20*) to final R_{cryst} = 20.4% and R_{free} = 28.3% (Table 2) (*14*).

Docking of the Transition State Analogue (TSA-1). The transition state analogue was built in Insight2000 (ACCELRYS, San Diego, CA) using cocaine coordinates (*15*) as a starting model. After addition of hydrogen atoms, the model was minimized with the Insight Discover module for 1000 iterations using X-plor potentials and the default parameters. These coordinates were used for docking with the program AUTODOCK, version 3.0 (*21*). In the docking simulation, the ligand was allowed to move within a cube with dimensions 25 Å per edge. The cube is subdivided into a grid with a 0.375 Å spacing between two grid points. This grid was centered on the approximate geometric center of the antibody hypervariable loops. The TSA-1 is placed at

Table 2: Final Data Collection and Refinement Statistics for 15A10

space group	$P2_1$
unit cell dimensions	$a = 37.5$ Å, $b = 108.4$ Å, $c = 111.3$ Å, $\beta = 90°$
resolution range (Å)	30−2.35 (2.45−2.35)[a]
observations	91 574
unique reflections	32 009
completeness (%)	85.4 (76.6)[a]
average I/σ_I	14.4 (2.8)[a]
R_{merge} (%)	8.3 (39.9)[a]
refined residues	854
refined water	108
twinned R_{cryst} (%)	20.4
twinned R_{free} (%)	28.3
Average *B* Values (Å^2)	
antibody	32
waters	40
Ramachandran Statistics	
most favored	81.3%
additional allowed	16.8%
generously allowed	1.7%
disallowed	0.3%
Deviations from Ideal Geometry (RMS)	
bond lengths	0.008 Å
bond angles	1.5°
dihedrals angles	27.7°
improper angles	0.99°

[a] Values in parentheses denote outer shell statistics.

an arbitrary position within the grid prior to docking. All flexible torsion angles in the TSA-1 were allowed to rotate freely, and for simplicity, the full Fab was truncated to the variable domains only. After docking, 100 solutions were clustered in groups with RMS deviations less than 1.5 Å. The groups were ranked by the docking energy, where the most favorable binding modes correspond to the group with the lowest docking energy. Altering the initial placement of the TSA-1 within the grid has no effect on the final docking result.

Chemical Modification of Side Chains and Activity Assays. Chemical Modification. Arginine residues were modified in a reaction containing 4 μM antibody, 90 μM phenylglyoxal, and 40 mM Na_3PO_4, pH 7.5, overnight at 23 °C. Tyrosine residues were modified in a reaction containing 4 μM antibody, 90 μM tetranitromethane, 10% (v/v) dioxane, and 50 mM Tris, pH 8.0, for 1 h at 23 °C. Histidine residues were modified in a reaction containing 4 μM antibody, 45 μM diethylpyrocarbonate, and 40 mM Na_3PO_4, pH 7.0, for 1 h at 23 °C. Deactivated histidine residues were reactivated using hydroxylamine. The chemically modified antibodies were exchanged to PBS, pH 7.4, using PD-10 gel filtration columns (Pharmacia), Microcon-10 concentrators (Amicon), or both.

Activity Assay. Catalytic activity was determined by comparing modified and unmodified 15A10 at two protein concentrations. Corrections for background hydrolysis were made through identical reactions in the absence of antibody. All reactions were incubated overnight at 37 °C with 15 mM cocaine containing trace amounts of [^{3}H]-cocaine (*4*) in 0.1 M Na_2HPO_4, pH 8.0. Acidification with cold HCl (aq) was followed by partition with hexane/diethyl ether (1:1) to separate cocaine from the products of hydrolysis. Protein concentrations of the final samples were determined using the BCA protein assay (Pierce) with BSA as a standard.

Cloning and Expression of the 15A10 Single Chain. The single-chain antibody (ScFv) was cloned using the pCANTAB 5E phagemid kit (Pharmacia Biotech). In this format, the carboxyl terminus of the variable heavy (V_H) chain is linked to the amino terminus of the variable light (V_L) chain by a 16 residue $(SGGGG)_3S$ linker sequence. In brief, mRNA from antibody-producing hybridomas was harvested and used as a template to generate cDNA that was PCR-amplified with random hexamer primers. The resulting clones were displayed on phage and screened for binding to the cocaine transition state analogue (Figure 1). ScFv was expressed as a fusion protein containing a cleavable N-terminal PelB leader sequence, which targets the ScFv for secretion to the periplasmic space for oxidative refolding, and a C-terminal E-tag, for both purification and detection. Positive clones were expressed as soluble ScFv, purified by affinity chromatography and assayed for catalytic activity against cocaine.

Site-Directed Mutagenesis. Point mutants were constructed by overlap extension PCR (*22*). The 5′ sense primers used for mutagenesis are listed; bold font corresponds to the codon that was mutated, and the numbering scheme follows the convention of Kabat and Wu for antibody sequences (*23*): AspL30Asn, GACTATTACAAGT**AAT**AACTATGC; TyrL32Phe, AAGTGATAAC**TTT**GCCAACTGGG; AsnL34Gln, GATAACTATGCC**CAA**TGGGTCC; AsnL34Gly, CTATGCC**GGC**TGGGTCCAAG; TrpL91Ala, CTGTGCTCTA**GCG**TACAGCAAC; HisL95Ser, GTACAGCAAC**AGC**TGGGTGTTC; TrpL96Ala, GCAACCAC**GCG**GTGTTCGGT; AspH31Asn, CATTCACT**AAC**TACAATATGTACTG; TyrH32Phe, CATTCACTGAC**TTC**AATATGTACTG; AsnH33Ala, CACTGACTAC**GCT**ATGTACTGGG; TyrH35Phe, CAATATG**TTC**TGGGTGAAGC; TyrH50Phe, GGATGGCA**TTT**ATTGATCCTTC. The plasmid-encoded primers used for initial amplification and subsequent extension reactions were 5′ sense CCATGATTACGCCAAGCTTTGGAGCC and 5′ antisense CGATCTAAAGTTTTGTCGTCTTTCC. Subsequently, the PCR products were subcloned into the original pCANTAB 5E plasmid via the *Sfi*I and *Not*I restriction sites. The desired mutations were confirmed by DNA sequencing. The ScFv mutants were overexpressed in *Escherichia coli* HB2051, and the protein was extracted from the periplasm by osmotic shock using 2 M sucrose. The ScFv was purified by affinity chromatography using an anti-E-tag mAb, and the buffer was exchanged to PBS, pH 7.4, using a PD10 desalting column.

Activity Assay. The cocaine hydrolysis reactions contained 5 μg of ScFv and 2 mM cocaine with a trace amount of ^{3}H-cocaine (*4*) in PBS, pH 7.4, in a total volume of 100 μL. A separate set of assays containing TSA-1 as an inhibitor was run to assess the contribution of spontaneous cocaine hydrolysis to the catalyzed reaction. The reactions were incubated at 37 °C for 18 h and stopped by addition of 100 μL of 0.1 N HCl. The substrate and products were separated in anion-exchange columns (Supelco, Bellefonte, PA) by washing initially with 2 mL of water to elute the reaction products followed by 3 mL of 0.2 N NaOH to elute substrate. The radioactive content of the fractions was measured on a scintillation counter, and relative activity was calculated from the ratio between products and substrate.

Determination of Binding to TSA by Enzyme-Linked Immunosorbent Assay (ELISA). Microtiter plates (Costar)

were coated for 2 h at 37 °C with 10 μg mL^{-1} TSA tethered to ovalbumin in PBS and blocked for 1 h at 37 °C with 1% BSA in PBS. Serial dilutions of purified ScFv in wash buffer (0.4% BSA, 0.05% Tween-20 in PBS) were added to the plates in triplicate and incubated for 1 h at room temperature. The plates were washed and incubated for an additional hour with 1:1000 dilution of secondary anti-E-tag antibody conjugated to horseradish peroxidase (Pharmacia). Subsequently, the substrate (1-Step ABTS, Pierce) was added, and absorbance values were measured at 405 nm on a plate reader.

RESULTS

Overview of the Crystal Structure. Antibody 15A10 consists of an IgG_1 heavy chain and λ light chain, which is a little unusual since λ chains comprise less than 5% of the entire murine light chain pool (*24*, *25*). The light chain of 15A10 is encoded by germline gene IGλV1 (*26*). The crystal structure of catalytic antibody 15A10 was determined by molecular replacement from data that exhibited an unusual form of pseudomerohedral twinning (*14*). Nevertheless, the structure was successfully refined with final $R_{cryst} = 20.4\%$, $R_{free} = 28.3\%$, and twinning fraction of 0.43 (Table 2). Two Fab molecules were found in the asymmetric unit. These NCS-related molecules superimpose closely with a backbone RMSD of 0.79 Å for V_L, 0.75 Å for V_H, and 0.82 Å overall. The light and heavy chain variable domains for each molecule bury a similar amount of surface area (1260 and 1245 Å^2 (*27*)) and form a similar number of contacts (122 and 112 contacts (*28*)) upon association. These values are within the normal range for V_L and V_H interfaces (*29*).

Light-Chain CDR Loops. The loops of the complementarity-determining region (CDR) are denoted as L1, L2, and L3 and H1, H2, and H3 for the light and heavy chains, respectively. CDRL1 contains a three-residue insertion, forming the usual combination of type I β-turn followed by an irregular helical segment (*30*) closely resembling a known canonical structure (*31*).

In κ and λ light chains, CDRL2 forms a totally conserved, classic γ-turn at position 51 (*31*). In one of the molecules in the asymmetric unit, the electron density was marginal from residues 50−54, so the backbone ϕ,ψ angles could not be accurately modeled. In the second molecule, the electron density was much clearer. However, definitive assignment of the ψ torsion at position 50 was not possible. According to the current model, this stretch of sequence (residues 49−52) resembles a type I′ β-turn, rather than a γ-turn (*32*). The observed structural deviation from the γ-turn could be due to a deviation in the primary sequence; normally, the sequence for this loop is GGTNNRAP (residues 49−56) (*23*), while the sequence of 15A10 is GVNNYRPP. Moreover, the two molecules in the asymmetric unit differ from one another in how CDRL2 interacts with CDRL1 and CDRH3. In the first molecule, the backbone nitrogen of ValL50 forms a H-bond to the carbonyl of GlyH97 in CDRH3. In the second molecule, the same backbone nitrogen instead forms a H-bond with the carbonyl of AlaL33.

CDRL3 forms an extended structure that approximates a known canonical structure. The only residues that differ from the canonical conformation are SerL93 and AsnL94 near the tip, but such variability at these positions is not uncommon (*31*). The sequence of this loop contains TrpL91 and TrpL96, which line one side of the binding pocket (Figure 2).

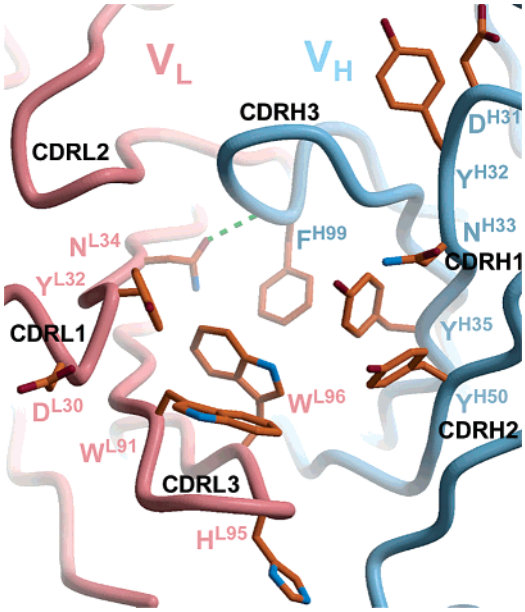

FIGURE 2: Top view (stereo) of the 15A10 binding pocket. The heavy chain is shown in blue and light chain in salmon. Hydrogen bonds are represented as green dashed lines. This coloring scheme will be used throughout. AsnH33, TyrH35, and TrpL96 cluster together to form the putative oxyanion hole. The side chain of AsnL34 forms a stabilizing hydrogen bond with the backbone of the CDRH3 loop.

Heavy-Chain CDR Loops. CDRs H1 and H2 both exhibit standard canonical structures. CDRH1 projects several hydrogen-bond-donating and -accepting side chains (AsnH33 and TyrH35) into the binding pocket, which may be of mechanistic significance (Figure 2).

CDRH3 is truncated compared to most other antibodies with a single deletion at position 100. The torso of CDRH3 contains the characteristic β-bulge consistent with the presence of ArgH94 and absence of AspH101 (*33*). CDRH3 was unexpectedly well-ordered in the electron density, considering that the loop contains three consecutive glycine residues at the apex (sequence CARGGGLFAFW). This unusual stretch of glycines probably arises from excision of the D_H gene, during $V_H-D_H-J_H$ recombination, and the N addition of eight guanine nucleotides. The evident conformational stability of CDRH3 is likely related to several key intraloop and interloop hydrogen bonds occurring between CDRH3 and H1, L1, and L2.

Architecture of the Binding Pocket. The binding pocket is largely hydrophobic, lined at the bottom and three sides by aromatic side chains (Figure 2); PheH99 constitutes the floor of the pocket, while TyrL32, TrpL91, TrpL96, TyrH35, and TyrH50 form three of the sides (Figure 2). The fourth side of the pocket is derived from the peptide backbone of CDRH3, as the residues of H3 are either glycine (H95−H97), alanine (H93, H101) or have side chains outside of the pocket (ArgH94, LeuH98, PheH102). The only cluster of hydrogen-bond-donating residues within the binding pocket is located on the heavy-chain side of the binding pocket and consists of AsnH33, TyrH35, TyrH50, and TrpL96 (Figure 2). These side chains are ideally situated to coordinate a tetrahedral transition state and, thus, are hypothesized to comprise the relevant portion of the binding pocket for catalysis.

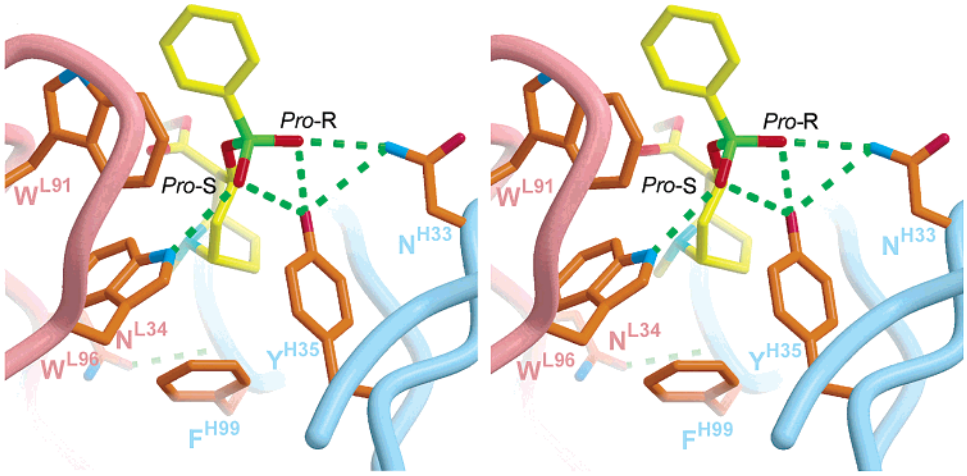

FIGURE 3: Side view (stereo) of the 15A10 binding pocket with TSA-1 docked. The TSA-1 is highlighted by brighter coloration; the phosphate is colored green. TrpL91 and TrpL96 form one side of the binding pocket, while PheH99 forms the floor of the binding pocket. TrpL96, TyrH35, and AsnH33 are perfectly arranged to coordinate the tetrahedral phosphonate.

Docking of the TSA-1. Superposition of the Lowest-Energy Cluster. Unfortunately, attempts to cocrystallize or soak preexisting crystals with transition state analogue have not been successful, possibly due to partial occlusion of the binding pocket by a symmetry-related molecule. Thus, docking of the ligand was assayed as an alternative means of analyzing and interpreting the available structural and biochemical data.

One hundred solutions from the docking simulation were clustered in groups with RMS deviations less than 1.5 Å. These groups were ranked according to favorable docking energy. The final solutions from docking are independent of initial starting conditions, as altering the initial placement and orientation of the TSA-1 within the binding pocket has little effect on the final docking result. Of the 100 solutions, nine were clustered at the lowest docking energy (predicted -10.1 kcal mol^{-1}). Superposition of these nine solutions shows that the main source of variation is in the torsion of the TSA-1 phenyl ring. Overall, the remaining phosphonate, methylester, and tropane skeleton superimpose closely. One of these solutions has been chosen for discussion (Figure 3), although the interactions described would apply to the other nine members of this cluster.

Chemical Modification. Arginine, histidine, and tyrosine residues were chemically modified to assess their contribution to hydrolytic activity. Modification of arginine guanidinyl groups with phenylglyoxal produced no change in Mab 15A10 catalytic activity, consistent with the structural data that show ArgH94 is outside the binding pocket. Tyrosine is abundantly distributed throughout the CDR regions of both the light and heavy chain of Mab-15A10. Activity was reduced to that of a noncatalytic control upon modification of tyrosine hydroxyl groups with tetranitromethane, underscoring the importance of the tyrosine hydroxyls observed in the binding pocket. A single histidine residue is located on CDRL3 and points out of the binding pocket (Figure 2). Surprisingly, activity was decreased to 6−12% after modification of imidazole groups with diethylpyrocarbonate (DEPC). DEPC is highly reactive and is known to react promiscuously with primary amino groups, cysteine and, notably, tyrosine (*34*), which might explain the decrease in activity. Hydroxylamine restored activity to 71.0−83.3% of baseline by deprotecting the DEPC-modified residues. Hydroxylamine had no affect on the activity of unmodified 15A10.

Table 3

ScFv construct	CDR	TSA-1 contact[a]	activity[b] (%)	TSA binding
wild-type		NA	100	+
AspL30Asn	L1	−	100	+
TyrL32Phe	L1	+	100	+
AsnL34Gly	L1	+	0	−
AsnL34Gln	L1	+	0	−
TrpL91Ala	L3	+	0	±
HisL95Ser	L3	−	0	+
TrpL96Ala	L3	+	3	±
TrpL96His	L3	+	0	−
AspH31Asn	H1	−	100	+
TyrH32Phe	H1	−	100	+
AsnH33Ala	H1	+	0	−
TyrH35Phe	H1	+	24	+
TyrH50Phe	H2	−	83	+

[a] Predicted contact based on computational docking. [b] The activity of mutants is calibrated against wild-type, which is defined as 100%. The cocaine concentration is 2 mM in these assays.

Mutagenesis. The ScFv retained similar kinetic parameters as the intact IgG after correcting for the number of binding sites, validating the construct design (data not shown). A panel of mutations was generated using the ScFv to determine side-chain contributions to activity as well as binding of TSA (Table 3). In general, mutation of residues with side chains directed away from the binding pocket had little effect on activity or TSA binding. For example, AspL30Asn and AspH31Asn retained full activity and TSA binding. The one exception was HisL95Ser, which lost activity but retained TSA binding. Mutation of TyrL32Phe (L1), TyrH32Phe (H1), or TyrH50Phe (H2) had no significant effect on hydrolytic activity or binding to TSA (Table 3). However, TyrH35Phe resulted in a marked decrease in activity (75% lower than the wild-type antibody) but without change in TSA binding. The AsnH33Ala mutant resulted in a total loss of hydrolytic activity and affinity for TSA. Two tryptophan residues (TrpL91 and TrpL96) are located toward the bottom and side of the binding pocket and appear to be critical in creating the hydrophobic environment required for accommodating the TSA in the cavity. Both TrpL91Ala and

TrpL96Ala mutants also resulted in a total loss of TSA affinity and catalytic activity (Table 3). The TrpL96His mutant was characterized, since histidine, in principle, might retain similar steric properties but provide a better general base and thereby facilitate catalysis. However, this substitution resulted in a total loss of catalytic activity and TSA affinity. The mutants AsnL34Gly and AsnL34Gln near the bottom of the binding pocket exhibit no catalytic activity and do not bind the TSA (Table 3). AsnL34 may fine-tune transition state binding by stabilizing the conformation of CDRH3 through the hydrogen-bond interaction with the backbone amide of PheH99.

DISCUSSION

Identification of the Putative Oxyanion Hole. In the crystal structure, the side chains of AsnH33, TyrH35, TyrH50, and TrpL96 are all located on one face of the binding pocket, and their side-chain hydrogen-bond-donating groups cluster in close proximity (Figures 2 and 3). Docking of the transition state analogue supports the hypothesis that AsnH33, TyrH35, and TrpL96 donate hydrogen bonds to the *Pro*-R, *Pro*-R/S, and *Pro*-S oxygens of the phosphonate, respectively (Figure 3). TyrH35 may form a bifurcated hydrogen bond to both the *Pro*-R and *Pro*-S oxygens. This docking result correlates well with chemical modification and mutagenesis studies (Table 3). Modification of tyrosine residues with tetranitromethane was detrimental to activity, and the mutations AsnH33Ala, TyrH35Phe, and TrpL91Ala either abolish or significantly affect both activity and TSA binding (Table 3). Thus, docking and mutagenesis imply that these residues comprise the portion of the binding pocket most important for transition state stabilization.

Orientation of the TSA in the Antibody Active Site. The docking simulation predicts that the lowest-energy conformation occurs when the TSA-1 is oriented in the binding pocket with the methylester and phenyl rings directed toward solution (Figure 3), reminiscent of the orientation seen in the cocaine-binding antibody, GNC92H2 (*15*). Here, the transition state analogue is predicted to form nearly the same number of contacts to both the light and heavy chains with the side chains of TyrL32, AsnL34, TrpL91, TrpL96, TyrH35, TyrH50, and PheH99 and the backbone of GlyH95, GlyH96, GlyH97, and LeuH98 (Figures 2 and 3). Importantly, these proposed interactions are consistent with mutagenesis data; residues that are not predicted to contact the TSA-1 (outside the binding pocket) have less of an impact on TSA binding and catalysis than residues inside the binding pocket (Table 3, Figures 2 and 3). The one exception in this trend is the HisL95Ser mutant, which is inactive yet outside the binding pocket (Figure 2). We speculate that HisL95 may form an important secondary sphere interaction (*35*) that has a subtle structural role.

While hydrogen-bonding interactions are relatively straightforward to predict due to their specificity and the requisite tetrahedral geometry of the phosphonate, the precise location of the tropane skeleton and phenyl ring is more difficult to predict. One unfortunate limitation of docking is that movements of the antibody side chains are not modeled. Thus, the orientation of the tropane skeleton and phenyl ring could be (and are likely) shifted in the true complex.

Proposed Mechanism for Catalysis. The close agreement between transition state stabilization, $K_M K_{DTS}^{-1}$, and the observed rate acceleration, $k_{cat}k_{uncat}^{-1}$ (Table 1), implies that hapten-binding interactions resemble the interactions found in the transition state and that binding energy is converted into catalysis with ~100% efficiency (*11*). The simplest mechanism for catalysis that is supported by our data is oxyanion stabilization resulting from attack by hydroxide. Although a pH−rate profile has not been measured for 15A10, many esterolytic antibodies show linear first-order reaction kinetics with respect to hydroxide anion concentration (*36*). Consequently, the attacking hydroxide is unlikely to be further activated by a general acid/base found in the antibody binding pocket. Indeed, with the exception of TyrH35, there is no other potential general acid/base in the binding pocket of 15A10. Rather, hydrogen bonds from the oxyanion hole to the carbonyl oxygen of the benzoyl ester of cocaine likely destabilize the ester making it more susceptible to attack by ambient hydroxide, while additional hydrogen bonds from the oxyanion hole preferentially stabilize the tetrahedral intermediate. Further structural studies are required to determine the precise direction of water attack with respect to the benzoyl ester.

Oxyanion stabilization has a differential impact on catalysis for various natural esterase and protease enzymes with estimated contributions of 2−3 kcal mol^{-1} in papain (*37*) and cutinase (*38*), 3−4 kcal mol^{-1} in prolyloligopeptidase (*39*), 2−5 kcal mol^{-1} in subtilisin (*40*−*42*), and 5−7 kcal mol^{-1} in acetylcholinesterase (*43*) and Zn^{2+} peptidase (*44*). A contribution of 5−7 kcal mol^{-1} from oxyanion stabilization was estimated for the D2.3 hydrolytic antibody (*36*). For 15A10, transition state stabilization is ~6 kcal mol^{-1} ($\Delta G_{cat}^{\ddagger} - \Delta G_{uncat}^{\ddagger} = RT(\ln(k_{cat}k_{uncat}^{-1}))$). Hydrolysis of cocaine above background was not detected for the AsnH33Ala mutant. If this mutant forms the H-bond in the oxyanion hole as predicted by docking, then its contribution to oxyanion stabilization is estimated to be at least 3−4 kcal mol^{-1}. The contribution from TyrH35 would be less since the activity of TyrH35Phe was only reduced ~4-fold compared to wild-type, unless a water molecule is able to compensate in some capacity for the absent hydroxyl, as was noted in prolyloligopeptidase (*39*). Prolyloligopeptidase also has a tyrosine hydroxyl in the oxyanion hole, but the Tyr473Phe mutant shows a modest 8−40-fold reduction in $k_{cat}K_M^{-1}$ (*39*). The contribution to oxyanion stabilization from TrpL96 is not straightforward to estimate, since this residue probably also plays an important role in substrate binding.

Comparison of 15A10 to Other Relevant Structures. Cocaine-Binding Antibody GNC92H2. Comparison of the cocaine-binding antibody GNC92H2 with the cocaine-degrading antibody 15A10 reveals several striking differences. At the level of primary sequence, the two antibodies share only 47% identity in the heavy chain and 40% identity in the light chain (Figure 4). At the structural level, the TSA-1 in 15A10 is proposed to form a nearly equal number of contacts with the light and heavy chain, while contacts in GNC92H2 were predominantly derived from the light chain (*15*). In addition, the binding pocket of 15A10 is shallower than that of GNC92H2. For GNC92H2, the tropane skeleton is buried more deeply in the pocket forming a contact with the side chain of GluH93, while in 15A10 PheH99 forms the floor of the binding pocket, which is located on the same level as H95 in GNC92H2. Moreover, the lack of side chains

Alignment for Heavy Chain

```
                1                   10                  20
15A10:  Q V K L Q Q S G P E L V K P G A S V K V S C K A S G Y
92H2:   E . Q . . . . . . . . K . . . E T . . I . . . T . . .

                30                  40                  50      a
15A10:  S F T D Y N M Y W V K Q N H G E S L E W I A Y I D P S
92H2:   . . . N . G . N . . . . A P . K G . K . M G W . N T Y

                        60                  70                  80
15A10:  N G D T F Y N Q K F Q G K A T V T L D K S S S T A F M
92H2:   T . E P T . A D D . R . R F A F S . A T . A . . . Y L

                    a b c               90                  100
15A10:  H L N S L T S E D S A V Y Y C A R G G G L F - A F W G
92H2:   Q I I N . K N . . T . T . F . E T Y D S P L G D Y . .

                    110
15A10:  Q G T T V T V S S
92H2:   . . . . . . . . .
```

Alignment for Light Chain

```
                1                   10                  20
15A10:  Q A V V T Q E S A - L T T S P G E T V T L T C R S S T
92H2:   D I G L . . S P . S . A V . L . Q R A . I S . . A . K

                a b c d     30                  40                  50
15A10:  G T I - T S D N Y A N W V Q E K P D H L F S G L I G V
92H2:   S V S T S G Y . . M H . . . Q . . G Q P P K L . . Y L

                            60                  70
15A10:  N N Y R P P G V P A R F S G S L T G D K A V L T I T G
92H2:   A S N L A S . . . . . . . . . G S . T D F T . N . H P

                    80                  90          a       100
15A10:  A Q T E D E A I Y F C A L W Y S N H - W V F G G G T K
92H2:   V E E . . A . T . Y . L Y S R E F P P . T . . . . . .

15A10:  L T V L G
92H2:   . E I K R
```

FIGURE 4: Sequence alignment of 15A10 with GNC92H2. The shaded regions correspond to the CDR loops. The sequence identity for both heavy and light chains is only ~47% (heavy chain) and ~40% (light chain). Thus, the two antibodies have little in common at the sequence and structural level, even though they were raised against similar haptens.

at the apex of CDRH3 (three glycines) and the single deletion (residue H100) in CDRH3 reduce the length of the loop compared to most other antibodies, further contributing to the relative shallowness of the pocket. Despite this shallowness, 15A10 could form as many contacts with the TSA-1 as GNC92H2 does with cocaine due to extensive interactions with the aromatic side chains in 15A10 (Figure 3).

A much more striking difference between the two antibodies is the apparent lack of electrostatic complementarity in the binding pocket of 15A10 compared to GNC92H2. The tropane nitrogen of cocaine has a p$K_a \approx 8.6$, which implies that it should be protonated at physiological pH. The binding pocket of GNC92H2 accommodates this positive charge with a corresponding negatively charged GluH93, which is buried at the bottom of the pocket (*15*). The binding pocket of 15A10, however, is lined with aromatic residues and lacks any electrostatic complementarity (Figure 5). Possibly, these aromatic residues (PheH99 and TrpL96) form stabilizing cation$-\pi$ interactions (*45*). Since AsnL34 is located at the floor of the 15A10 binding pocket, in proximity to the proposed position for the tropane skeleton, it would be interesting to test an AsnL34Asp mutation to see whether electrostatic complementarity can be engineered into the

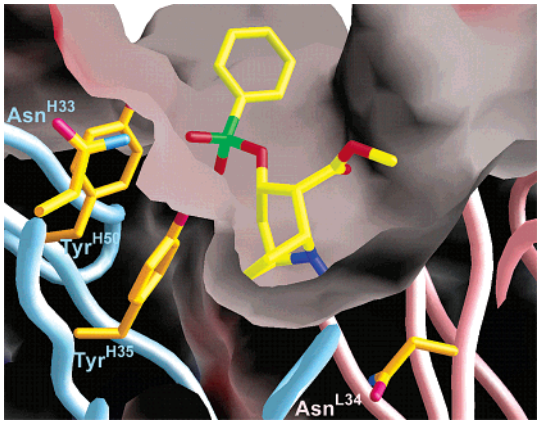

FIGURE 5: Electrostatic complementarity surface of binding pocket. A red or blue surface would correspond to electronegative or electropositive potential, respectively. Here, the predominant gray coloration indicates that the pocket is hydrophobic, due to the aromatic side chains lining the interior of the pocket. AsnH33 and TyrH35 are proposed to form hydrogen bonds in the oxyanion hole.

15A10 binding pocket. Such complementarity might assist in lowering the K_M for the antibody, thereby improving the specificity constant. Finally, the total number of hydrogen

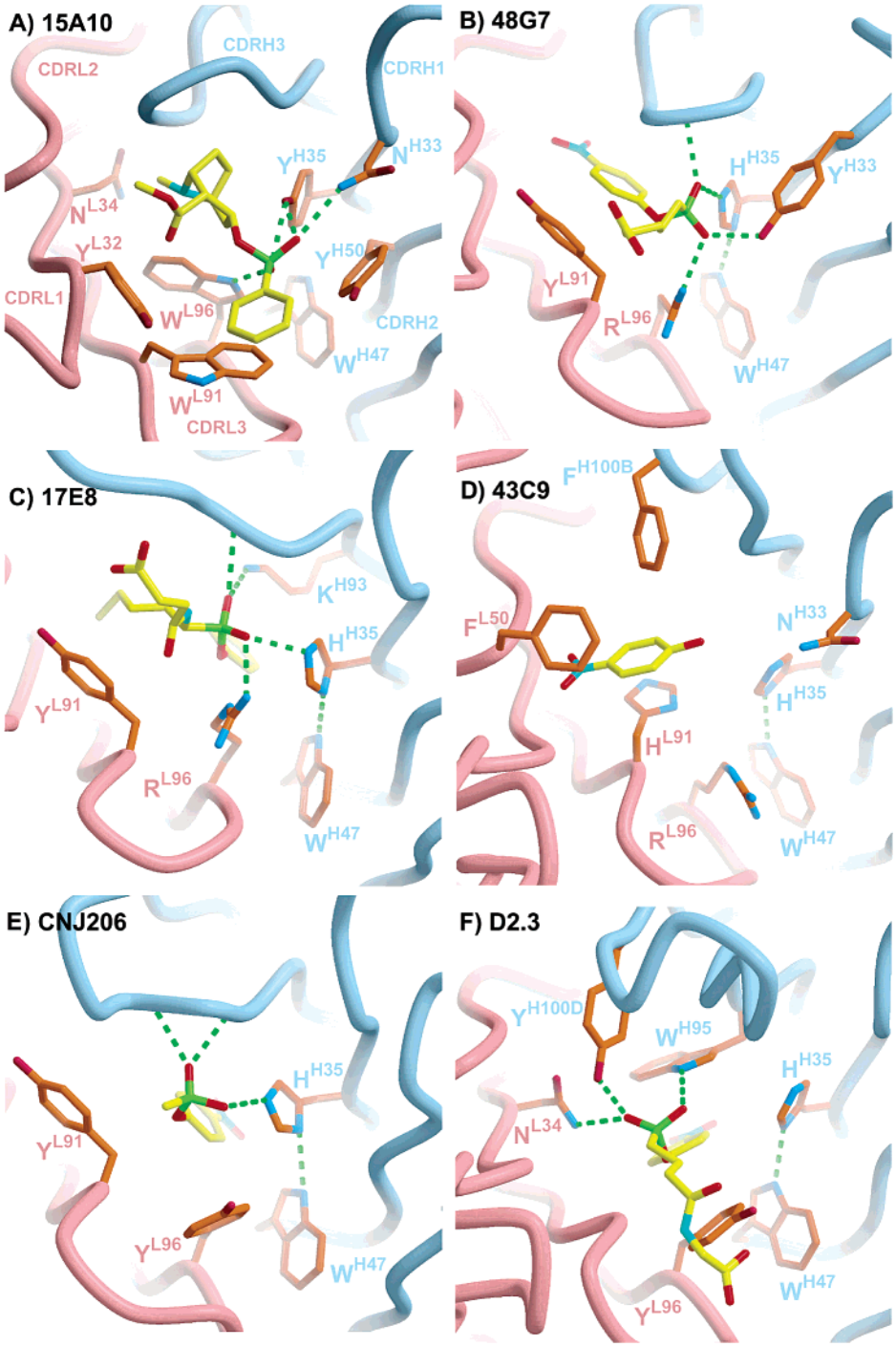

FIGURE 6: Comparison to other known hydrolytic antibodies. The variable framework regions of six different hydrolytic antibodies were aligned to the 15A10 crystal structure. Nearly the same view is shown in each example to illustrate the interactions with the TSA (when available) in the oxyanion hole. The conserved TrpH47 is shown in each panel as reference: (A) 15A10; (B) 48G7; (C) 17E8; (D) 43C9; (E) CNJ206; (F) D2.3.

bonds proposed to form between 15A10 and the TSA differs substantially from GNC92H2. Hydrogen bonds were noticeably absent from the GNC92H2 complex, and were limited to a water-mediated hydrogen bond between the antibody and cocaine (*15*).

Comparison to Other Hydrolytic Antibodies. Nearly half of the ~50 catalytic antibody structures deposited in the Protein Data Bank (PDB) are from various hydrolytic antibodies in complex with transition state analogues, substrate analogues, and products (Table 1). These antibodies include 48G7 (*46*, *47*), 17E8 (*48*), 29G11 (*49*), CNJ206 (*50*), 43C9 (*10*), D2.3 (*51*), and 6D9 (*52*). All of these antibodies were raised against either phosphonate or phosphonamidate transition state analogues and, with the exception of 6D9 (which will not be discussed further) (*52*), catalyze the hydrolysis of *p*-nitrophenol esters.

To gain greater insight to the catalytic mechanism for 15A10, these hydrolytic antibodies were superimposed according to their framework variable regions (Figure 6). Examination of these crystal structures reveals obvious similarities in the oxyanion hole of 15A10, 48G7, 17E8, 29G11, CNJ206, and 43C9 (Figure 6a−f). Antibody 48G7

utilizes ArgL96, TyrH33, HisH35, and the backbone amide of H96 for transition state stabilization (Figure 6b) (*46*, *47*). Antibodies 17E8 and 29G11 (Figure 6c,d) are related to each other (92% sequence identity (*53*)) and use similar residues for oxyanion stabilization (*48*, *49*) as 48G7, except that a hydrogen bond from the LysH93−Nz amine substitutes for the observed TyrH33 hydroxyl in 48G7. Antibody CNJ206 is also similar with hydrogen bonds from HisH35 and the backbone amides of H96 and H97 (Figure 6e) (*50*). Although a crystal structure of 43C9 in complex with the transition state analogue is not available, it is proposed that HisL91, ArgL96, AsnH33, and HisH35 likewise contribute to oxyanion stabilization (Figure 6f) (*10*). Therefore, for these antibodies the constellation of side chains derived from L96, H33, H35, and the backbone amide of H96 constitute a general recurring theme for oxyanion stabilization, arising from structural convergence within the antibody-binding pocket (*6*, *7*).

The proposed residues involved in oxyanion stabilization for 15A10 (TrpL96, AsnH33, and TyrH35) (Figure 6a) agree with the assignment for these other antibodies (48G7, 17E8, 29G11, CNJ206, and 43C9). Notably, 43C9 also has an asparagine at position H33 (Figure 6f). While the position of the oxyanion hole is predicted to be located in a similar area of the antibody-binding pocket, the precise identity of the residues differs. HisH35 is highly conserved in these other hydrolytic antibodies, while in 15A10, this residue is a tyrosine, and TrpL96 is more commonly an arginine.

Catalytic antibody D2.3 differs from this general theme (Figure 6g). Here, oxyanion stabilization arises from hydrogen bonds to AsnL34, TrpH95, and TyrH100D (*51*). While the location of these residues is on the opposite side of the binding pocket to the corresponding residues in 15A10, the identity of the residues is exactly the same as those proposed in 15A10 (Figure 6a). Thus, the composition of the oxyanion hole in D2.3 is quite similar to that proposed to form in 15A10, albeit on the opposite side of the binding pocket.

CONCLUSIONS

We have structurally and biochemically characterized a cocaine-degrading catalytic antibody that has been tested successfully in preclinical trials (*5*, *12*). The combination of TSA-1 docking in the crystal structure, chemical modification and mutagenesis data, and comparison to other hydrolytic antibodies collectively supports the proposed mechanism of oxyanion stabilization and the assignment of the oxyanion hole (AsnH33, TyrH35, and TrpL96). The crystal structure provides a basis for structure-based humanization, just as the structure of GNC92H2 facilitated its humanization (*17*). In addition, the structure provides a foundation for additional mutagenesis studies to enhance the catalytic activity. TrpL96Arg or TyrH35His would introduce oxyanion hole residues identical to those seen in the 48G7/17E8 family of hydrolytic antibodies. Likewise, AlaH93Lys would further mimic the oxyanion hole of 17E8 and 29G11 (Figure 6c). AsnL34Asp would provide greater electrostatic complementarity at the base of the binding pocket, which was an important determinant for recognition in the cocaine-binding antibody and, thus, could lower the K_M for 15A10. In this regard, it might be possible to introduce a bulky tryptophan residue at the apex of the CDRH3 loop to aid in capping the active site and thereby lower the K_M. Random mutagenesis of any of the proposed contact residues in CDRL1, L3, H1, and H3 and screening by phage display against the TSA could provide additional means of improving the catalytic activity (*35*, *54*, *55*). Finally, comparison of this cocaine catalytic antibody to others (as their structures become available) will provide insights into antibody engineering, as well as second-generation TSA design strategies.

ACKNOWLEDGMENT

The authors thank the Stanford Synchrotron Radiation Laboratory (SSRL) for support at beam line 9-2.

REFERENCES

1. Ritz, M. C., Lamb, R. C., Goldberg, S. R., and Kuhar, M. J. (1987) Cocaine receptors on dopamine transporters are related to self-administration of cocaine, *Science 237*, 1219−1223.
2. Carroll, F. L., Howell, L. L., and Kuhar, M. J. (1999) Pharmacotherapies for treatment of cocaine abuse: preclinical aspects, *J. Med. Chem. 42*, 2721−2736.
3. Landry, D. W., Zhao, K., Yang, G. X., Glickman, M., and Georgiadis, T. M. (1993) Antibody-catalyzed degradation of cocaine, *Science 259*, 1899−1901.
4. Yang, G., Chun, J., Arakawa-Uramoto, H., Wang, X., Gawinowicz, M. A., Zhao, K., and Landry, D. W. (1996) Anti-cocaine catalytic antibodies: a synthetic approach to improved antibody diversity, *J. Am. Chem. Soc. 118*, 5881−5890.
5. Mets, B., Winger, G., Cabrera, C., Seo, S., Jamdar, S., Yang, G., Zhao, K., Briscoe, R. J., Almonte, R., Woods, J. H., and Landry, D. W. (1998) A catalytic antibody against cocaine prevents cocaine's reinforcing and toxic effects in rats, *Proc. Natl. Acad. Sci. U.S.A. 95*, 10176−10181.
6. MacBeath, G., and Hilvert, D. (1996) Hydrolytic antibodies: variations on a theme, *Chem. Biol. 3*, 433−445.
7. Tantillo, D. J., and Houk, K. N. (2001) Canonical binding arrays as molecular recognition elements in the immune system: tetrahedral anions and the ester hydrolysis transition state, *Chem. Biol. 8*, 535−545.
8. Gigant, B., Charbonnier, J.-B., Eshhar, Z., Green, B. S., and Knossow, M. (1997) X-ray structures of a hydrolytic antibody and of complexes elucidate catalytic pathway from substrate binding and transition state stabilization through water attack and product release, *Proc. Natl. Acad. Sci. U.S.A. 94*, 7857−7861.
9. Resmini, M., Vigna, R., Simms, C., Barber, N. J., Hagi-Pavli, E. P., Watts, A. B., Verma, C., Gallacher, G., and Brocklehurst, K. (1997) Characterization of the hydrolytic activity of a polyclonal catalytic antibody preparation by pH-dependence and chemical modification studies: evidence for the involvement of Tyr and Arg side chains as hydrogen-bond donors, *Biochem. J. 326*, 279−287.
10. Thayer, M. M., Olender, E. H., Arvai, A. S., Koike, C. K., Canestrelli, I. L., Stewart, J. D., Benkovic, S. J., Getzoff, E. D., and Roberts, V. A. (1999) Structural basis for amide hydrolysis catalyzed by the 43C9 antibody, *J. Mol. Biol. 291*, 329−345.
11. Stewart, J. D., and Benkovic, S. J. (1995) Transition-state stabilization as a measure of the efficiency of antibody catalysis, *Nature 375*, 388−391.
12. Baird, T. J., Deng, S. X., Landry, D. W., Winger, G., and Woods, J. H. (2000) Natural and artificial enzymes against cocaine. Monoclonal antibody 15A10 and the reinforcing effects of cocaine in rats, *J. Pharmacol. Exp. Ther. 295*, 1127−1134.
13. Jarvik, M. E., and Schneider, N. G. (1992) in *Substance Abuse: a comprehensive textbook* (Lowinson, J. H., Ruiz, P., Millman, R. B., and Langrod, J. G., Eds.) pp 205−221, Williams and Wilkins, Baltimore, MD.
14. Larsen, N. A., Heine, A., de Prada, P., Redwan, R. M., Yeates, T. O., Landry, D. W., and Wilson, I. A. (2002) Structure determination of a cocaine hydrolytic antibody from a pseudomerohedrally twinned crystal, *Acta Crystallogr. D58*, 2055−2059.
15. Larsen, N. A., Zhou, B., Heine, A., Wirsching, P., Janda, K. D., and Wilson, I. A. (2001) Crystal structure of a cocaine-binding antibody, *J. Mol. Biol. 311*, 9−15.

16. Larsen, N. A., Turner, J. M., Stevens, J., Rosser, S. J., Basran, A., Lerner, R. A., Bruce, N. C., and Wilson, I. A. (2002) Crystal structure of a bacterial cocaine esterase, *Nat. Struct. Biol. 9*, 17−21.
17. Redwan, R. M., Larsen, N. A., Zhou, B., Wirsching, P., Janda, K. D., and Wilson, I. A. (2003) Expression and characterization of a humanized cocaine-binding antibody, *Biotech. Bioeng. 82*, 612−618.
18. Kissinger, C. R., Gehlhaar, D. K., and Fogel, D. B. (1999) Rapid automated molecular replacement by evolutionary search, *Acta Crystallogr. D55*, 484−491.
19. Herbst-Irmer, R., and Sheldrick, G. M. (1998) Refinement of twinned structures with SHELXL97, *Acta Crystallogr. B54*, 443−449.
20. Brünger, A. T., Adams, P. D., Clore, G. M., Delano, W. L., Gros, P., Grosse-Kunstleve, R. W., Jiang, J.-S., Kuszewski, J., Nilges, M., Pannu, N. S., Read, R. J., Rice, L. M., Simonson, T., and Warren, G. L. (1998) Crystallography & NMR System: A new software suite for molecular structure determination, *Acta Crystallogr. D54*, 905−921.
21. Morris, G. M., Goodsell, D. S., Halliday, R. S., Huey, R., Hart, W. E., Belew, R. K., and Olson, A. J. (1998) Automated docking using a Lamarckian genetic algorithm and empirical binding free energy function, *Comput. Chem. 19*, 1639−1662.
22. Ho, S. N., Hunt, H. D., Horton, R. M., Pullen, J. K., and Pease, L. R. (1989) Site-directed mutagenesis by overlap extension using the polymerase chain reaction, *Gene 77*, 51−59.
23. Kabat, E. A., Wu, T. T., Perry, H. M., Gottesman, K. S., and Foeller, C. (1991) *Sequences of proteins of immunological interest*, 5th ed., National Institutes of Health, Bethesda, MD.
24. McIntire, K. R., and Rouse, A. M. (1970) Immunoglobulin light chains: alteration of κ:λ ratio, *Fed. Proc. Fed. Am. Soc. Exp. Biol. 29*, 704.
25. Cotner, T., and Eisen, H. N. (1978) The natural abundance of λ2-lightchains in inbred mice, *J. Exp. Med. 148*, 1388−1399.
26. Lefranc, M. P., Giudicelli, V., Ginestoux, C., Bodmer, J., Muller, W., Bontrop, R., Lemaitre, M., Malik, A., Barbie, V., and Chaume, D. (1999) IMGT, the international ImMunoGeneTics database, *Nucleic Acids Res. 27*, 209−212.
27. Connolly, M. L. (1983) Analytical molecular surface calculation, *J. Appl. Crystallogr. 16*, 548−558.
28. Sheriff, S., Hendrickson, W. A., and Smith, J. L. (1987) Structure of myohemerythrin in the azidomet state at 1.7/1.3 Å resolution, *J. Mol. Biol. 197*, 273−296.
29. Stanfield, R. L., Takimoto-Kamimura, M., Rini, J. M., Profy, A. T., and Wilson, I. A. (1993) Major antigen-induced domain rearrangements in an antibody, *Structure 1*, 83−93.
30. Wu, S., and Cygler, M. (1993) Conformation of complementarity determining region L1 loop in murine IgG lambda light chain extended the repertoire of canonical forms, *J. Mol. Biol. 229*, 597−601.
31. Al-Lazikani, B., Lesk, A. M., and Chothia, C. (1997) Standard conformations for the canonical structures of immunoglobulins, *J. Mol. Biol. 273*, 927−948.
32. Richardson, J. S. (1981) The anatomy and taxonomy of protein structure, *Adv. Protein Chem. 34*, 167−339.
33. Morea, V., Tramontano, A., Rustici, M., Chothia, C., and Lesk, A. M. (1998) Conformations of the third hypervariable region in the V_H domain of immunoglobulins, *J. Mol. Biol. 275*, 269−294.
34. Krell, T., Chackrewarthy, S., Pitt, A. R., Elwell, A., and Coggins, J. R. (1998) Chemical modification monitored by electrospray mass spectrometry: a rapid and simple method for identifying and studying functional residues in enzymes, *J. Pept. Res. 51*, 201−209.
35. Arkin, M. R., and Wells, J. A. (1998) Probing the importance of second sphere residues in an esterolytic antibody by phage display, *J. Mol. Biol. 284*, 1083−1094.
36. Lindler, A. B., Kim, S. H., Schindler, D. G., Eshar, Z., and Tawfik, D. S. (2002) Esterolytic antibodies as mechanistic and structural models of hydrolases − a quantitative analysis, *J. Mol. Biol. 320*, 559−572.
37. Menard, R., Carriere, J., Laflamme, P., Plouffe, C., Khouri, H. E., and Vernet, T. (1991) Contribution of the glutamine 19 side chain to transition-state stabilization in the oxyanion hole of papain, *Biochemistry 30*, 8924−8928.
38. Nicolas, A., Egmond, M., Verrips, C. T., de Vlieg, J., Longhi, S., Cambillau, C., and Martinez, C. (1996) Contribution of cutinase serine 42 side chain to the stabilization of the oxyanion transition state, *Biochemistry 35*, 398−410.
39. Szeltner, Z., Renner, V., and Polgar, L. (2000) Substrate- and pH-dependent contribution of oxyanion binding site to the catalysis of prolyl oligopeptidase, a paradigm of the serine oligopeptidase family, *Protein Sci. 9*, 353−360.
40. Bryan, P., Pantoliano, M. W., Quill, S. G., Hsiao, H.-Y., and Poulos, T. (1986) Site-directed mutagenesis and the role of the oxyanion hole in subtilisin, *Proc. Natl. Acad. Sci. U.S.A. 83*, 3743−3745.
41. Carter, P., and Wells, J. A. (1990) Functional interaction among catalytic residues in subtilisin BPN′, *Proteins: Struct., Funct., Genet. 7*, 335−342.
42. O'Connell, T. P., Day, R. M., Torchilin, E. V., Bachovchin, W. W., and Malthouse, J. G. (1997) A 13C-NMR study of the role of Asn-155 in stabilizing the oxyanion of a subtilisin tetrahedral adduct, *Biochem. J. 326*, 861−866.
43. Harel, M., Quinn, D. M., Nair, H. K., Silman, I., and Sussman, J. L. (1996) The X-ray structure of a transition state analog complex reveals the molecular origins of the catalytic power and substrate specificity of acetylcholinesterase, *J. Am. Chem. Soc. 118*, 2340−2346.
44. Phillips, M. A., Fletterick, R., and Rutter, W. J. (1990) Arginine 127 stabilizes the transition state in carboxypeptidase, *J. Biol. Chem. 265*, 20692−20698.
45. Gallivan, J. P., and Dougherty, D. A. (1999) Cation-pi interactions in structural biology, *Proc. Natl. Acad. Sci. U.S.A. 96*, 9459−9464.
46. Wedemayer, G. J., Wang, L. H., Patten, P. A., Schultz, P. G., and Stevens, R. C. (1997) Crystal structures of the free and liganded form of an esterolytic catalytic antibody, *J. Mol. Biol. 268*, 390−400.
47. Wedemayer, G. J., Patten, P. A., Wang, L. H., Schultz, P. G., and Stevens, R. C. (1997) Structural insights into the evolution of an antibody combining site, *Science 276*, 1665−1669.
48. Zhou, G. W., Guo, J., Huang, W., Fletterick, R. J., and Scanlan, T. S. (1994) Crystal structure of a catalytic antibody with a serine protease active site, *Science 265*, 1059−1064.
49. Buchbinder, J. L., Stephenson, R. C., Scanlan, T. S., and Fletterick, R. J. (1998) A comparison of the crystallographic structures of two catalytic antibodies with esterase activity, *J. Mol. Biol. 282*, 1033−1041.
50. Charbonnier, J. B., Carpenter, E., Gigant, B., Golinelli-Pimpaneau, B., Eshhar, Z., Green, B. S., and Knossow, M. (1995) Crystal structure of the complex of a catalytic antibody Fab fragment with a transition state analog: structural similarities in esterase- like catalytic antibodies, *Proc. Natl. Acad. Sci. U.S.A. 92*, 11721−11725.
51. Charbonnier, J. B., Golinelli-Pimpaneau, B., Gigant, B., Tawfik, D. S., Chap, R., Schindler, D. G., Kim, S. H., Green, B. S., Eshhar, Z., and Knossow, M. (1997) Structural convergence in the active sites of a family of catalytic antibodies, *Science 275*, 1140−1142.
52. Kristensen, O., Vassylyev, D. G., Tanaka, F., Morikawa, K., and Fujii, I. (1998) A structural basis for transition-state stabilization in antibody-catalyzed hydrolysis: crystal structures of an abzyme at 1.8 Å resolution,*J. Mol. Biol. 281*, 501−511.
53. Guo, J., Huang, W., Zhou, G. W., Fletterick, R. J., and Scanlan, T. S. (1995) Mechanistically different catalytic antibodies obtained from immunization with a single transition-state analog, *Proc. Natl. Acad. Sci. U.S.A. 92*, 1694−1698.
54. Baca, M., Scanlan, T. S., Stephenson, R. C., and Wells, J. A. (1997) Phage display of a catalytic antibody to optimize affinity for transition-state analog binding, *Proc. Natl. Acad. Sci. U.S.A. 94*, 10063−10068.
55. Takahashi, N., Kakinuma, H., Liu, L., Nishi, Y., and Fujii, I. (2001) In vitro abzyme evolution to optimize antibody recognition for catalysis, *Nat. Biotech. 19*, 563−567.
56. Stewart, J. D., Krebs, J. F., Siuzdak, G., Berdis, A. J., Smithrud, D. B., and Benkovic, S. J. (1994) Dissection of an antibody-catalyzed reaction, *Proc. Natl. Acad. Sci. U.S.A. 91*, 7404−7409.
57. Patten, P. A., Gray, N. S., Yang, P. L., Marks, C. B., Wedemayer, G. J., Boniface, J. J., Stevens, R. C., and Schultz, P. G. (1996) The immunological evolution of catalysis, *Science 271*, 1086−1091.

BI049495L